Energy modelling and emissions analysis of indoor-grown produce for Arctic Canada

Carsen Banister[1], Adam Wills[1], Koreen Legaspi[2], Travis Moore[1]
[1]National Research Council Canada, Ottawa, Canada
[2]University of Waterloo, Waterloo, Canada

Abstract

Many remote communities rely heavily on shipped-in goods due to limited or no local availability. Communities in Canada that are not road-connected require air transport of fresh produce. As a result of food security issues, there is interest in exploring applications of controlled environment agriculture (CEA) in the Arctic and there is no prior work on energy or emissions analysis. This work estimates the emissions of a modelled CEA enclosure operated in the Canadian Arctic. Several scenarios are considered, which have varying capacities of small wind turbines, solar photovoltaic panels, and battery energy storage and range from 29 to 82% renewable fraction. A range of emissions intensities result, which highlight both the potential and challenges for renewable energy in Arctic applications.

Introduction

Food insecurity is a complex and interdisciplinary topic for Arctic communities. Inuit and other Indigenous people have sustained themselves from their surrounding natural environments for millennia. Although country food (food harvested from the surrounding environment) remains an important part of the diet for cultural, cost, and security reasons, grocery store food has become another important source of food in the Arctic over the 20th century. Given that polar climates are incompatible with most farming food production, food other than country food is transported in from southern Canada. Non-perishable foods are shipped via sea lift as much as possible and perishable foods are transported via air.

Food costs at stores in the Arctic are more than double that in southern Canada and many items are in excess of quadruple the cost. Perishable foods tend to have the highest mark-up because they cannot be shipped by sea lift. These foods are important sources of micronutrients, but can often be overlooked because of the high cost and poor quality due to the additional transportation time to the Arctic. To increase the quality, affordability, and security of nutritious food in Canada's Arctic, there is interest in exploring options food local produce growth. Due to the high reliance on fossil fuels for heat and electricity in remote northern locations within Canada, the energy demands and associated emissions are of concern. A small controlled environment agriculture (CEA) facility and energy systems to support its operation are modelled in TRNSYS 18 to quantify the energy and emissions performance and explore the fuel and emission reductions that are possible with small wind and solar photovoltaic (PV) systems.

Literature Review

In one of the earliest related studies, the Defence and Civil Institute of Environmental Medicine (1978) within Defence Research and Development Canada (DRDC) proposed the feasibility of developing an air-transportable, hydroponic growth module for producing vegetables all-year in remote communities in northern Canada. Greenhouse gas emissions were not considered in the analysis; however, a cost comparison was presented. While flying in produce from southern Canada was estimated to cost $0.36 per capita per week, the construction, implementation, and operation & maintenance costs for locally producing an equivalent amount of food were estimated at $0.85 per capita per week. This suggests that the energy demands and associated costs from lighting and heating for this system were high in comparison to the alternative.

Avard (2015) studied the potential of northern greenhouses as a key approach for addressing food security in Inuit communities, particularly through the Kuujjuaq Greenhouse Project in Nunavik. Results indicate positive impacts in food security, sustainability, and socioeconomics and demonstrate the interest and need for northern greenhouses and agriculture for food sovereignty and resilience in the north.

Sipola (2019) illustrated the social, nutritional, and ecological impact of local food systems in Indigenous, Arctic communities made by northern gardens and greenhouses. Through a case study of a greenhouse development in Kuujjuaq, Nunavik, Sipola examined the environmental and sustainable challenges of greenhouse development. Despite the required transportation of soil and use of fossil fuels for greenhouse heating, there is interest for local non-profit development of gardening and greenhouses in the Canadian Arctic that promotes communal learning while introducing fresh produce yield. However, the work highlights the implications of exogenous, non-collaborative development and over-

innovation when addressing sustainable food production and sovereignty.

Chen & Natcher (2019) developed an inventory and examination of 38 community gardens and greenhouses in northern Canada. A subset of these projects were highlighted to demonstrate their benefits, including local food production and skill development in the community. The community gardens and greenhouses are examples of an effective strategy for food sovereignty because of the reduced dependency on expensive, nutrient-poor food imports and ability to satiate food needs in remote communities.

Ljungqvist et al. (2021) proposed using excess heat from a data center as a heating source for producing tomato crops in 2000 m^2 and 10 000 m^2 greenhouses in northern Sweden (65°N). A building energy model of the data center and the greenhouse was developed considering lighting, temperature, transpiration, ventilation, and cost. Results of the simulation concluded that approximately 90% of the heating demand could be met for the small greenhouse and 55% for the large could be met from the excess heat.

The majority of the local food growth operations in the Canadian north are based on greenhouses. There are some indoor food growth operations in existence and interest is increasing. Overall, Avard, Sipola, and Chen validate the multi-disciplinary facet of designing an indoor grow container, particularly relating to the social, cultural, and nutritional considerations of growing food in Arctic communities. No published work similar to the analysis presented here has been found to exist.

Methodology

This section outlines the methodology used to estimate the emissions produced from growing produce locally in a controlled environment. This analysis enables a comparison of the carbon emissions of each scenario and identification of reasonable renewable energy fraction targets for northern food growth in a controlled environment. To understand the emissions associated with local produce growth in Arctic communities, an indoor grow container and off-grid energy system was designed and modelled in TRNSYS 18, as shown in Figure 1. The model is configured to run for one simulated year and operates under the following assumptions:

- The container and materials are located in the Arctic community of Cambridge Bay, Nunavut.
- Although lighting needs vary over a plant's growing cycle, a uniform light schedule is used throughout.
- Water pump electrical loads trays are neglected.
- Equipment and supplies transportation emissions are neglected.
- Crops are assumed to achieve optimal yield.

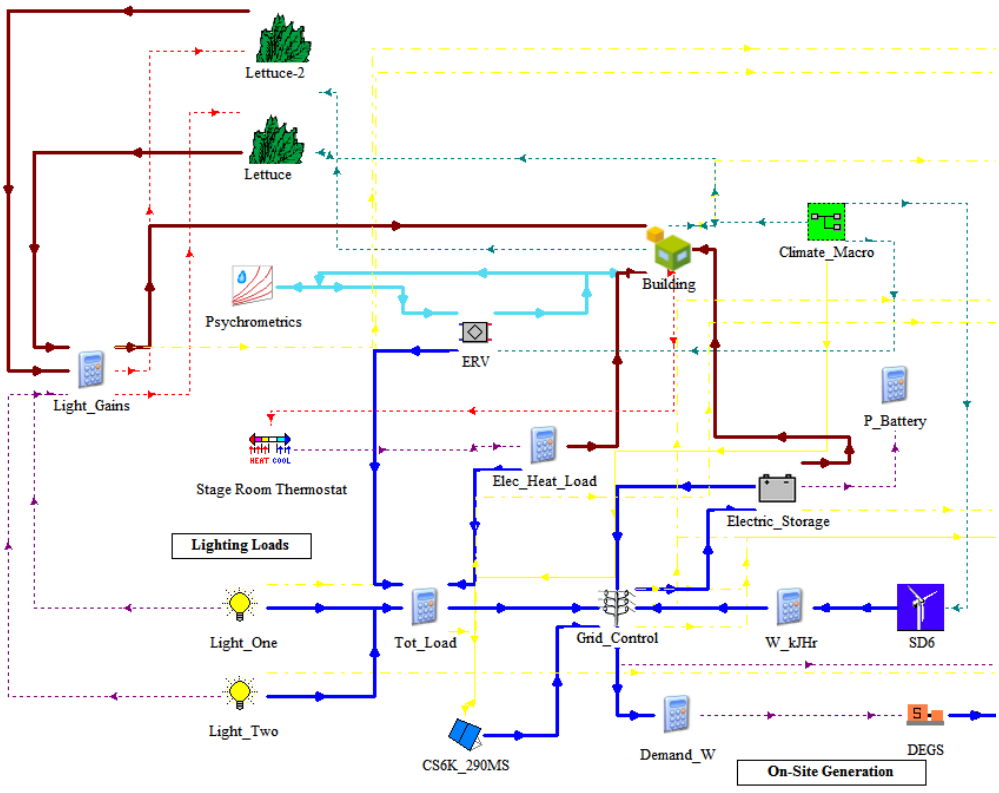

Figure 1. Overview model developed for the analysis in TRNSYS 18

Model Components

Climate. TRNSYS standard library Type 15 (TESS, 2019) was used to load annual climate data into the model. In this simulation study, the annual hourly Canadian Weather Year for Energy Calculations (CWEC) data file for Cambridge Bay, NU from Environment and Climate Change Canada was used (ECCC, 2021). Type 15 linearly interpolates to determine sub-hourly conditions for dry-bulb temperature, relative humidity, and wind speed and direction. Sub-hourly solar radiation is processed using the hourly solar intensity values available in the climate file and solar processing algorithms from Duffie & Beckman (2006).

Wind Turbine. The wind turbine was modelled using TRNSYS standard library Type 90 (TESS, 2019), labelled as "SD6" in Figure 1. Type 90 is an empirical steady-state model which uses manufacturer reported test data to model turbine power output and performance under different environmental operating conditions. The power versus output curve under standard testing conditions forms the primary model for the turbine. The SD6 turbine is a three-blade horizontal axis turbine with a swept area of 23.7 m^2. Standard test data for the SD6 turbine was obtained from the Small Wind Certification Council (ICC-SWCC, 2019). Figure 2 plots the turbine power output versus wind speed at the hub height from ICC-SWCC (2019). The curve represents performance with a turbine inlet air density of 1.225 kg/m^3.

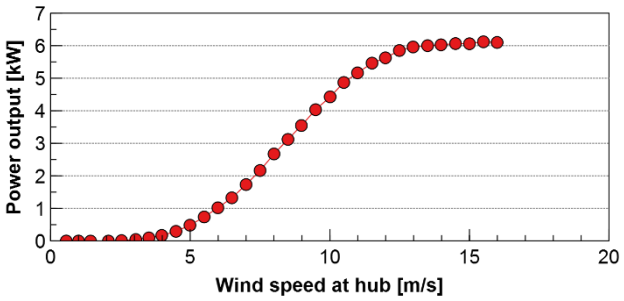

Figure 2. SD6 wind turbine power output versus wind speed at hub, data from ICC-SWCC (2019)

The Type 15 "Weather" component in Figure 1 provides the climate inputs of wind speed, ambient dry-bulb temperature, and barometric pressure to the wind turbine model. Table 1 provides a summary of the most pertinent wind turbine model parameters.

Table 1. Summary of wind turbine model parameters

Parameter	Value
Rotor height [m]	9.0
Rotor diameter [m]	5.6
Rated power [kW]	5.2
Rated wind speed [m/s]	11.0

Additional details of the wind turbine model are omitted here for clarity, and the interested reader is directed to TESS (2019) for additional information.

Solar Photovoltaic Panels. Solar photovoltaic (PV) panels were modelled using Type 190c, a validated empirical steady-state model of PV modules developed by De Soto et al. (2006). This five-parameter model approximates system operating performance by representing PV modules as resistance-diode circuits. The panels modelled are based on 290 W modules from Canadian Solar (2018). The parameters used are listed below in Table 2.

Table 2. Summary of PV module model parameters

Parameter	Value
Short-circuit current at STC, I_{SC} [A]	9.67
Open-circuit voltage at STC, V_{OC} [V]	39.3
Voltage at maximum power point and STC, V_{MPP} [V]	32.1
Current at maximum power point and STC, I_{MPP} [A]	9.05
Temperature coefficient of I_{SC} at STC [A/K]	0.004835
Temperature coefficient of V_{OC} at STC [V/K]	-0.11397
Number of cells wired in series	60
Extinction coefficient-thickness product of cover	0.013
Module area [m^2]	1.457
Five Parameters	
Ideality factor, a [-]	1.576
Light current, I_L [A]	9.682
Diode reverse saturation current, I_0 [A]	1.413E-10
Series resistance, R_s [Ω]	0.2735
Shunt resistance, R_{sh} [Ω]	219.2

Battery. The battery system was modelled using TRNSYS standard library Type 47 (TESS, 2019), illustrated in Figure 1 as "Electric_Storage". For the purposes of this study, the base transient energy balance algorithm is used. This approach uses a basic energy in, out, and stored balance as the simulation progresses. To account for system energy transfer and storage inefficiencies, a constant charging efficiency is defined for the model. This parameter acts as a proxy for "round-trip" battery charge/discharge. It is realized as a loss in the model during charge of the battery only; there is no constant trickle of standby loss during idle operation or losses during discharge. This is likely implemented in this way to simplify the simulation of transient operation and control of the battery.

Given the simplicity of the model, it may be considered agnostic to battery technology type. The charging efficiency was assumed to be 90% based on assumed round-trip efficiency of lithium-ion batteries reported by Brown

(2018). The key battery model parameters are summarized in Table 3.

Table 3. Summary of battery model parameters

Parameter	Value
Cell energy capacity [Wh]	3000
Cells in parallel	1, 2, or 4
Cells in series	4
Charging efficiency [%]	90.0

Further details of the battery model are omitted here for brevity, and the interested reader is directed to TESS (2019) for additional information. It was assumed that the battery and various micro-grid system components were housed in the agriculture container, and that losses from battery charging are passed as thermal gains to the enclosure.

Diesel Generator. The diesel generation system was modelled using TRNSYS standard library Type 120 (TESS, 2019). This is a steady-state empirical performance map model. The model is constructed around a part-load ratio to fuel consumption rate curve. Based on input from project partners, a 7.6 kW_e diesel generation system (Hatz Diesel, 2020) was to be installed at the site. Using manufacturer performance data the performance curve in Figure 3 was defined.

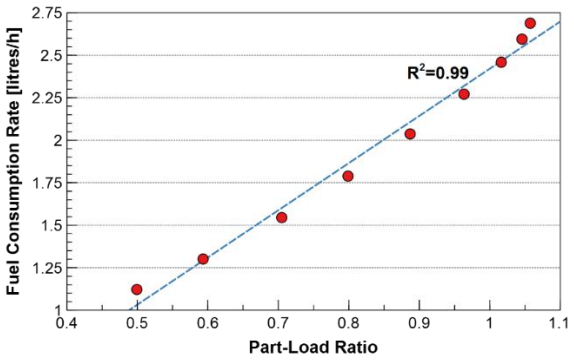

Figure 3. Diesel generator part-load versus fuel consumption, based on data from Hatz Diesel (2020)

The manufacturer reported fuel consumption in grams per kWh versus power output. To convert to the model required units of litres per hour shown in Figure 3, a diesel fuel density of 833 grams per litre was assumed. This was based on data from ISED (2018) for diesel fuel at 25 °C, which was the ambient test conditions reported by the manufacturer. Figure 3 shows that the performance curve can be accurately approximated using a linear regression, with a coefficient of determination, R^2, of 0.99. While a second-order polynomial was found to more precisely capture the manufacturer reported data points in Figure 3, the model implementation is limited to linear expressions of performance curves. The salient model parameters are summarized in Table 4.

Table 4. Summary of diesel generator model parameters

Parameter	Value
Maximum electrical generation capacity [kW]	7.9
Minimum electrical generation capacity [kW]	3.9
Rated electrical generation [kW]	7.6
Performance curve slope [g/litre/PLR]	2.777
Performance curve intercept [g/litre]	-0.356

Operation of the diesel generator is governed by the grid controller, described in the following subsection. For each time step, the controller passes a power demand to the diesel generator. If this demand is below the minimum operating threshold of the generator, the generator operates at its minimum output capacity and excess electrical generation is re-directed by the grid controller to charge the battery system or to an electrical load dump on the AC bus as a last resort. Similarly, if demand exceeds maximum capacity the generator operates at its maximum capacity point and additional energy is assumed to be drawn from an external electrical grid. The diesel generator is assumed to be housed in an enclosure which is separate from the agriculture container.

Grid Controller. Basic and fit-for-purpose grid control types are available in TRNSYS standard and extended libraries. A new Type needed to be implemented to manage the modelled energy system of Figure 1. The goal of the new algorithm design was such that it would meet the needs of the current modeling study and be generic enough to be applied to a multitude of future micro-grid simulation research studies. Figure 4 illustrates the micro-grid configuration the controller algorithm is designed to manage.

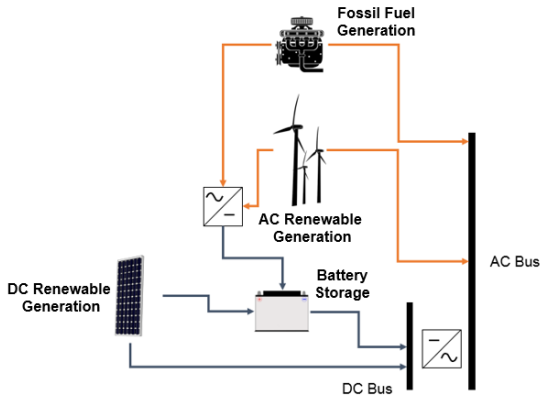

Figure 4. Micro-grid configuration assumed by controller

Illustrated as "Grid_Ctl" in Figure 1, the grid control type acts as the central hub of the system energy model. At each simulation time step, AC and DC generation output, battery

state-of-charge (SOC), and total site AC demand are taken as inputs to determine dispatch and control action. The grid controller algorithm also models the performance of the DC-to-AC inverter and AC-to-DC rectifier shown in Figure 4. Both devices are modelled assuming user-prescribed constant conversion efficiencies.

The primary priority of the control algorithm was to first supply all on-site renewable generation to concurrent site demands. This choice was based on the philosophy that on-site generation is better utilized by directly supplying concurrent loads rather than being stored which incurs charge, discharge, and standby losses. If there is insufficient or no available renewable generation during a period of demand, the battery is then discharged if there is sufficient capacity. Capacity is determined by the battery's SOC and also by a maximum power draw limit specified by the user. If there is no capacity in the battery to meet the load, or the demand is greater than the maximum the battery can provide, the battery is dispatched to provide the maximum power it is able to deliver and the remainder of the demand is requested by the grid controller to the diesel generation.

It was stated previously that the diesel generator can only be operated between maximum and minimum power outputs. The grid controller is aware of these limitations since these limits are passed to the controller as parameters. Therefore, if the request to the diesel generator is greater than the capacity of the generator, the controller accounts for this deficit by allocating that deficit to being supplied by an external source. If the demand is below the lower operating limit of the generator, the generator is set to run at its minimum operating point and the excess generation is used to charge the micro-grid battery system, illustrated as the connection between the fossil fuel generator and battery system via the rectifier in Figure 4. The controller parameters are summarized in Table 5.

Table 5. Summary of grid controller model parameters

Parameter	**Value**
High limit of battery SOC [%]	98
Low limit of battery SOC [%]	20
Battery output power capacity [kW]	10.8
Charge SOC threshold [%]	N/A
Inverter efficiency [%]	95
Rectifier efficiency [%]	95

The grid controller maintains a range of battery bank SOC based on the high and low limits described in Table 5. The high limit of 98% was implemented instead of 100% for stability in the model. The low limit of 20% was selected to reflect a common 80% depth-of-discharge (DoD) used by manufacturers to rate the cycle life of the batteries. Battery output capacity was selected based on typical manufacturer-reported maximum continuous charge and discharge rates.

The charge SOC threshold was a parameter implemented in the control algorithm to include functionality present in the TRNSYS standard library grid controller Type 48. While not used in this simulation, this threshold can specify a limit where if the battery bank is below the SOC threshold and starts charging, then it must continue charging until the SOC of the battery meets the threshold. Otherwise if the battery bank is discharging and passes below the threshold, it can keep discharging to its low limit of battery SOC. This enables an additional limit on deep discharge of the battery while still making capacity available during high periods of demand.

Building Model and System Loads. The CEA building enclosure is composed of two side-by-side 20 foot shipping containers with overall outside dimensions of 20' long x 16' wide x 8' 6" high. The container has a south-facing 7' 8" x 7' 6" door and 2' x 4' triple-glazed window, as shown in Figure 5. The geometry was modelled using SketchUp and TRNSYS3D, a SketchUp plugin for TRNSYS to model multi-zone buildings. Using WINDOW 7.8, the window was modelled as three layers of LoE 116 on 3mm clear glass, with 12 mm gaps of 10% Air/90% Argon mix, resulting in a centre of glass U-value of 0.633 $W/m^2 \cdot K$ and solar heat gain coefficient of 0.081, with a vinyl frame of U-Value of 1.7 $W/m^2 \cdot K$.

The geometry was imported into TRNBuild, a TRNSYS interface used to modify building model characteristics, to further develop the non-geometric properties of the building model. The building envelope was defined according to the layers detailed in Table 6, with the objective of optimizing the insulation of the grow container while limiting to a reasonable thickness. The building model is included as a Type 56 component.

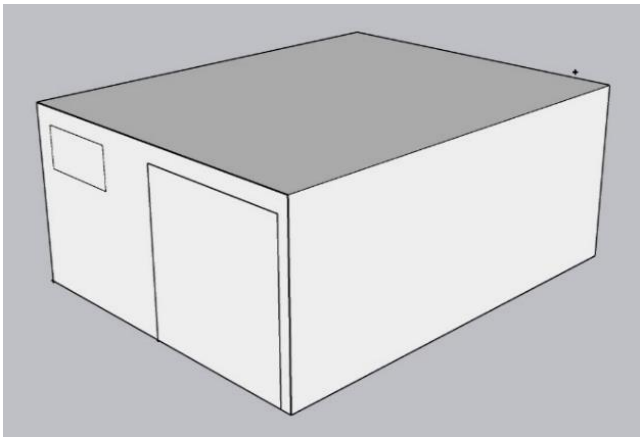

Figure 5. Grow Container geometry modelled in SketchUp

Table 6. Construction materials of container

Building Component	Layer (Exterior to Interior)	Material Property			Thickness [m]	Overall U-Value [W/m²·K]	Convective Heat Transfer Coeffecient [kJ/h·m²·K]	
		Conductivity [kJ/h-m-K]	Capacity [kJ/kg-K]	Density [kg/m³]			Inside	Outside
Wall	Steel	163	0.5	7824	0.002	0.227	22.5	120
	Polyisocyanurate	0.13	1.5	30	0.153			
Roof	Steel	163	0.5	7824	0.002	0.227	32.7	120
	Polyisocyanurate	0.13	1.5	30	0.153			
Floor	Terrazzo	6.48	0.79	2560	0.025	0.195	22.5	120
	Extruded Polystyrene	0.108	1.5	33	0.051			
	Plywood	0.432	1.21	544	0.019			
	Batt Insulation	0.18	0.96	19	0.147			
	Plywood	0.432	1.21	544	0.019			

The HVAC system includes a dual-stage electric resistance heater and a 22.5 W variable-speed fan to control the ambient temperature and ventilation of the container. The fan is modelled using Type 147 and varies from a minimum speed of 100 CFM, a first speed of 120 CFM, and a second speed of 140 CFM. The infiltration rate of outdoor air into the container is set to be 0.21 ACH, aligning with the National Energy Code of Canada for Buildings (NECB) regulation in NECB 2017: A-8.4.3.3.(3). The container's temperature is monitored and controlled by a stage room thermostat as detailed in Table 7. The controller is modelled using Type 108 and based on temperatures determined to be appropriate values for plant growth identified by literature of similar existing grow systems.

Table 7. Thermostat sepoints

Thermostat Input	Temperature [°C]
1st stage heating set point	18
2nd stage heating set point	15

The container has six electrical loads: the 22.5 W variable-speed fan, the electric space heater, LED grow lamps (48 fixtures at 70W each), a 27.7W circulation fan, a 240W load for data acquisition hardware and sensors, and 75W of standby power drawn from the inverter and rectifier. To reduce the peak load caused by lighting, the lighting schedule follows a half on/half off cycle every twelve hours. The lighting power density was specified in consultation with a plant agriculture colleague at National Research Council Canada.

The heat gains of the container are contributed to by the container's electric space heating, the lighting loads, the plants' sensible and latent heat losses, and the batteries. The sensible and latent heat gained from the plant is modelled using a custom TRNSYS type developed by the project team and based on literature and an existing lettuce model developed by Talbot & Monfet (2020).

Emissions. A carbon dioxide equivalent emissions factor of 2.7 kilograms per Litre of diesel fuel combusted is assumed for a small diesel generator (ECCC, 2019). This figure is for combustion of the fuel only and neglects the emissions associated with extraction, transportation, storage, and distribution.

Agriculture Configuration. A representative configuration for an Arctic indoor grow environment was developed and is shown in Figure 6. The bottom half of the layout contains equipment and supplies and the top half of the layout contains the grow area. The total cultivation area of the grow container is 216 ft^2 or 20.1 m^2. The grow area is comprised of 9 shelf racks, each with three levels of 8 ft^2.

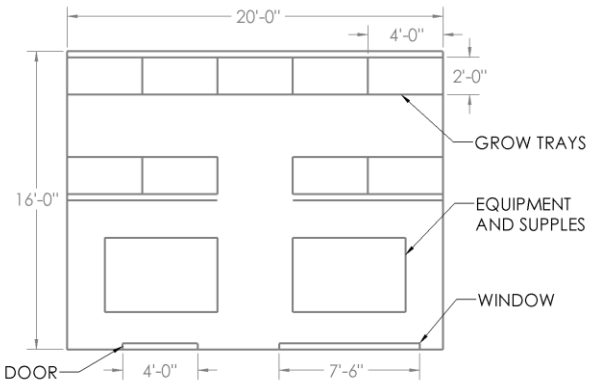

Figure 6. Proposed configuration of grow container

Plant Productivity

In terms of expected productivity, EDEN ISS Greenhouse's biomass production in Zabel et al. (2020) was referenced, which reported an edible produce weight per cultivation area of $1.56 \pm 0.12 (0.98\text{-}2.46)$ kg/m^2 for a Batavia lettuce crop. This equates to an average mass growth rate of approximately 0.043 $\frac{kg}{m^2 d}$. To compute a minimum expected

mass of fresh produce per cultivation area in the Arctic grow container, this study will assume the production of Batavia lettuce in the container, since the other reported crops have a higher produce weight per cultivation area.

Results and Discussion

The model was run for several cases of wind, solar, and battery capacities, which are outlined in Table 8. The base case (#1) for the analysis is all energy conversion being met by a small diesel generator. This case is very similar to community diesel generator systems meeting electricity demand in terms of emissions performance. The breakdown of annual demand by each load is shown in Figure 7, where it is clearly seen that the agriculture lighting is the majority of the demand at around 79%. The agriculture lighting offsets a major portion of what would be the heating demand as a result and mitigating overheating with ventilation is necessary during the warmest months. The space heating system is the second highest demand at 13% and the DAQ system is third at 5%.

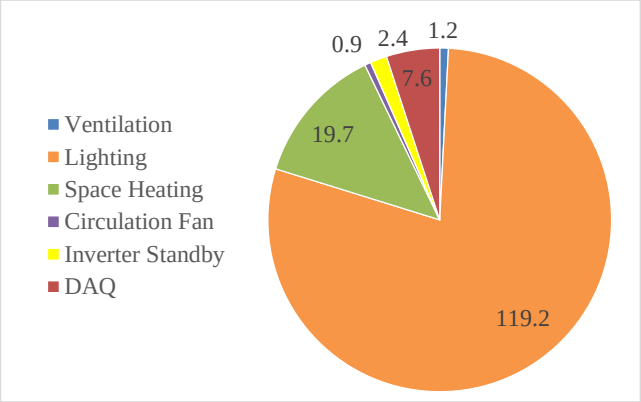

Figure 7. Annual load breakdown by end use for all simulations [GJ]

Looking at Table 8, the cases are arranged with increasing renewable energy capacity, and thus decreasing fuel use and emissions. As expected, the renewable energy dumped begins to rise substantially as the combined wind turbine and solar PV capacity goes well above 10 kW. Due to the sustained load of the agriculture lights, the need for battery storage is relatively low unless the renewable energy system capacity is very large. This is illustrated by the minimal difference in performance between cases # 3, 4, and 5.

Monthly electrical loads over the course of a year against a breakdown of the energy sources for the case of a single 5.2 kW wind turbine with 5.8 kW PV and 24 kWh of battery capacity (case #4) are presented in Figure 8. This shows the minimal quantity of renewable energy dumped due to a sufficiently high stable load from the agriculture lighting relative to the capacities of the renewable energy system. The wind turbine meets 29% of the demand from the load, while only 4% is dumped. The solar PV meets 16% of the demand with only 10% dumped. For reference, on April 1, 2022 diesel fuel in Nunavut for building use was $1.15 per litre outside of Iqaluit. However, prices typically remain constant for a year since fuel is only delivered in a 1-2 month window each year and fuel for delivery is secured well in advance. This relatively low price is based on fuel purchased in 2020 and 2021 during low oil prices.

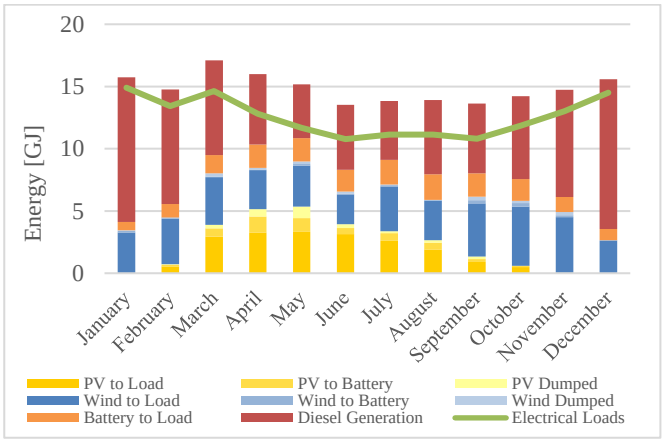

Figure 8. Monthly energy conversion and demand: 5.2 kW wind turbine, 5.8 kW solar PV, 24 kWh battery (case #4)

Table 8. Summary of key performance metrics for all cases simulated

Case #	Wind Turbine [kW]	Solar PV [kW]	Battery [kWh]	Renewable Fraction	Wind Dumped	Solar Dumped	Annual Diesel Fuel [L]	Annual Emissions [kg CO_2e]
1	-	-	24	-	-	-	12,337	33,310
2	5.2	-	24	29%	2%	-	8,793	23,741
3	5.2	5.8	12	42%	5%	16%	7,118	19,219
4	5.2	5.8	24	43%	4%	10%	6,973	18,827
5	5.2	5.8	48	44%	2%	6%	6,851	18,498
6	10.4	-	24	46%	20%	-	6,670	18,009
7	10.4	11.6	12	60%	26%	53%	4,992	13,478
8	10.4	11.6	24	63%	24%	45%	4,575	12,353
9	20.8	23.2	24	73%	51%	78%	3,389	9,150
10	20.8	23.2	48	82%	48%	68%	2,187	5,881

The final calculation of this study is to estimate the CO_2e emissions per quantity of produce based on the modeling results and production estimates from EDEN ISS presented in the Methodology. For a grow area of 20.1 m^2, the agriculture configuration presented in this analysis has the potential to grow 315 kg of lettuce per year. For case #4, this works out to 60 kg CO_2e per kg of produce.

The emissions analysis conducted for cases with modest renewables penetration shows that without significant clean energy penetration, the resulting emissions from CEA are very high. In comparison, estimated emissions for production of foods such as tomatoes, brassicas, and berries range from 0.2 to 2.1 kg CO_2e per kg of produce (Poore & Nemecek, 2018). However, these estimates do not include transportation, which could prove significant for air transport to the Arctic.

Conclusions

To investigate the energy requirements and resulting emissions from growing food indoors in the Arctic, a CEA and energy system were modeled in TRNSYS. As a result of the light requirements for plant growth, lighting was the predominant energy demand at over 75%. The heat produced by the lighting also supplied a significant portion of the space heating demand, which resulted in much lower space heating energy end-use.

Ten cases of varying small wind turbine and solar PV panel capacities were modeled. The modelled wind turbines provide approximately double the diesel fuel reduction than the solar PV panels over the course of a year per unit of rated power output. The wind turbines provide significantly more diesel fuel savings due to their much higher utilization throughout the course of the year.

These results from renewable energy simulation for building loads highlight the need for policies to enable small renewable energy systems in remote and northern communities to be grid-tied to maximize the proportion of renewable energy used. The cases with significant renewables penetration also have a significant amount of renewable energy generation dumped, which could otherwise displace diesel fuel use by other customers. The results from this study indicate significant renewable energy penetration is required for a site, community, or region to bring the emissions of CEA in the Canadian Arctic into a reasonable range.

Future Work

1. The emissions performance of CEA will be compared to the alternative of flying in food grown in lower latitudes.
2. The yield of other produce of interest may be explored. Fruit-bearing produce could reduce the carbon emissions per mass of produce significantly through higher weight yields.

Acknowledgements

Input on agricultural configurations from Shawn Clark of Aquatic and Crop Resource Development at National Research Council Canada is appreciated.

References

Avard, E. (2015). *Northern greenhouses: An alternative local food provisioning strategy for Nunavik*. Université Laval.

Brown, M. D. (2018). Simulation and Optimization of High-Penetration Wind and Solar Energy for the Canadian High Arctic Research Station.

Canadian Solar. (2018). *All-Black: CS6K-290|295|300MS*. Walnut Creek.

Chen, A., & Natcher, D. (2019). Greening Canada's Arctic food system: Local food procurement strategies for combating food insecurity. *Canadian Food Studies*, *6*(1), 144–154.

Defence and Civil Institute of Environmental Medicine. (1978). *Fesibility Study of an Arctic Food Producing Facility*. Downsview, Ontario.

Duffie, J. A., & Beckman, W. A. (2006). *Solar Engineering of Thermal Processes*. Hoboken: John Wiley & Sons, Inc.

ECCC. (2019). *Emission Factors Annex*. Retrieved from https://data.ec.gc.ca/data/substances/monitor/canada-s-official-greenhouse-gas-inventory/Emission_Factors.pdf

ECCC. (2021). Engineering Climate Datasets. Retrieved from https://climate.weather.gc.ca/prods_servs/engineering_e.html

Hatz Diesel. (2020). *Data sheet B-series*. Ruhstorf an der Rott.

ICC-SWCC. (2019). *Summary Report SWCC-11-04*. Brea.

ISED. (2018). Volume correction factors—diesel, bio-diesel and diesel blends. Retrieved January 11, 2022, from https://www.ic.gc.ca/eic/site/mc-mc.nsf/eng/lm00127.html

Ljungqvist, H. M., Mattsson, L., Risberg, M., & Vesterlund, M. (2021). Data center heated greenhouses, a matter for enhanced food self-sufficiency in sub-arctic regions. *Energy*, *215*, 119169.

Poore, J., & Nemecek, T. (2018). Reducing food's environmental impacts through producers and consumers. *Science*, *360*.

Sipola, S. (2019). *From Community Gardens to Hybrid Hydroponics: The evolution of northern greenhouses and Arctic gardening*. The Arctic University of Norway.

Soto, W. De, Klein, S. A., & Beckman, W. A. (2006). Improvement and validation of a model for photovoltaic array performance. *Solar Energy*, *80*, 78–88.

Talbot, M. H., & Monfet, D. (2020). Estimating the impact of crops on peak loads of a Building-Integrated Agriculture space. *Science and Technology for the Built Environment*, *26*(10), 1448–1460.

TESS. (2019). *TRNSYS 18 Mathematical Reference*. Madison.

Wills, A., Banister, C., Pellissier, M., & Berquist, J. (2021). A multi-year analysis of Canadian Arctic historical weather data in support of solar and wind renewable energy deployment. *E3S Web of Conferences*, *246*.

Zabel, P., Zeidler, C., Vrakking, V., Dorn, M., & Schubert, D. (2020). Biomass Production of the EDEN ISS Space Greenhouse in Antarctica During the 2018 Experiment Phase. *Frontiers in Plant Science*, *11*(May), 1–13.